

Metamirrors Based on Arrays of Silicon Nanowires with Height Gradients

Marinus A. Otte, Antonio Garcia-Martin, Xavier Borrise, and Borja Sepulveda*

Metamaterials are artificial constructs that have attracted intense attention in the photonics field for finding new ways to control light propagation and to achieve complex optical effects.^[1,2] To date, most metamaterials in the visible and near infrared regimes are based on arrays of nanosized metallic plasmonic elements. Such plasmonic metasurfaces have not only achieved a remarkable versatility to control the optical properties in surfaces but also shown interesting optical properties from the fundamental point of view, such as hyperbolic^[3,4] or epsilon-near-zero^[5] effective dielectric constants. Plasmonic metamaterials have also enabled modifying light orbital angular momentum^[6–8] as well as the generation of the spin Hall effect^[9] and have been already employed in actual applications such as holograms^[10,11] or wave retarders.^[12]

The careful spatial control of size, orientation, and shape of plasmonic nanostructures within the arrays has also been used to generate periodic phase gradients, which have given rise to the generalized Snell law to account for the anomalous reflection and refraction of light in this kind of metasurfaces.^[13] Such periodic phase gradients have been employed for the efficient coupling of light into surface modes^[14] and for the development of metalenses.^[15,16]

In the search of new metamaterials with low losses, high-index dielectric nanostructures exhibiting Mie resonances in the optical frequency range have emerged as a very appealing candidates.^[17,18] Silicon-based metamaterials have been the base to create phase gradients by changing the geometry and distribution of the nanostructures on the surface.^[19] Silicon metamaterials have demonstrated applications as axicons, blazed gratings, achromatic metasurfaces, and metalenses.^[20]

Current plasmonic and dielectric metamaterials have in common that the desired optical response is achieved by a careful choice of the lateral size, shape, orientation, and/or separation of the nanostructures on the surface. However, tailoring the vertical dimension of the nanostructures is generally cum-

bersome due to the technical complexity required to achieve high spatial resolution.

Herein we show that a careful design of the nanostructure height is indeed an efficient way to spatially tune the optical properties in high-index dielectric metamaterials. We demonstrate that arrays of silicon nanowires with tailored height gradients can generate phase gradients to develop metamirrors enabling light focusing in arbitrary shapes. In addition, the combination of height gradients and nanowires with anisotropic cross-section permits simultaneous light focusing and strong polarization conversion in the focused light. Such height-induced phase gradients can complement recently developed planar phase gradient metamaterials^[21,22] to achieve even stronger lensing effects.

We employ a recently developed fabrication method based on mechanically controlled metal-assisted chemical etching of silicon^[23] to obtain ordered arrays of Si nanowires with height gradients. This fabrication method makes use of a thin gold layer comprising an array of nanoholes as catalyst to etch the silicon substrate. During the etching process the catalytic metal mesh is plastically deformed, thereby generating the mechanical stress that spatially modulates the etching rate and gives rise to the array of nanowires with height gradients. The height gradients can be tuned by varying the stiffness of the catalytic metal mesh, i.e., by modifying the size and shape of the nanoholes array, the edge-to-edge separation distance between nanoholes, and the metal thickness. All the metamirrors shown in this work are produced using 20 nm thick gold films and the same etching conditions of ref.^[23], with an etching time of 2 min. The height gradients could be larger by increasing etching time and by designing rupture points in the catalytic metal film.^[23]

The Si nanowire metamirror concept is shown in **Figure 1a**, which displays a circular array of cylindrical nanowires with height gradients in the radial direction, i.e., the height of the nanowires increases toward the center of the array. In the fabricated example of **Figure 1b**, the diameter of the array is 10 μm , the pitch is 300 nm, and the nanowires height increases from zero at the border of the array, up to 500 nm at its center. In all the arrays in this work, the 20 nm Au film used for etching is kept at the bottom of the array to increase the reflectivity of the metamirror. In these arrays, the radial height variation is converted into a radial phase variation in the light reflected by the array, which strongly depends on the nanowire diameter and pitch.

As **Figure 1d** shows, such radial phase gradient enables tight focusing the reflected light within a spot with a focal length of 12 μm . Since the nanowires have circular cross-sections, the focusing effect in **Figure 1** is polarization insensitive. Similar focusing behavior can be theoretically observed in finite difference time domain (FDTD) calculations of circular arrays of cylindrical nanowires with equivalent radial height gradients.

Dr. M. A. Otte
Nanobiosensors and Bioanalytical Applications Group
Catalan Institute of Nanoscience and
Nanotechnology (ICN2)
CSIC, CIBER_BBN and The Barcelona Institute
Science and Technology
Campus UAB, Bellaterra, 08193 Barcelona, Spain



Dr. A. Garcia-Martin
IMM—Instituto de Microelectrónica de Madrid (CNM-CSIC)
Isaac Newton 8, PTM, Tres Cantos, E-28760 Madrid, Spain

Dr. X. Borrise, Dr. B. Sepulveda
Catalan Institute of Nanoscience and Nanotechnology (ICN2)
CSIC and The Barcelona Institute of Science and Technology
Campus UAB, Bellaterra, 08193 Barcelona, Spain
E-mail: borja.sepulveda@icn2.cat

DOI: 10.1002/adom.201600933

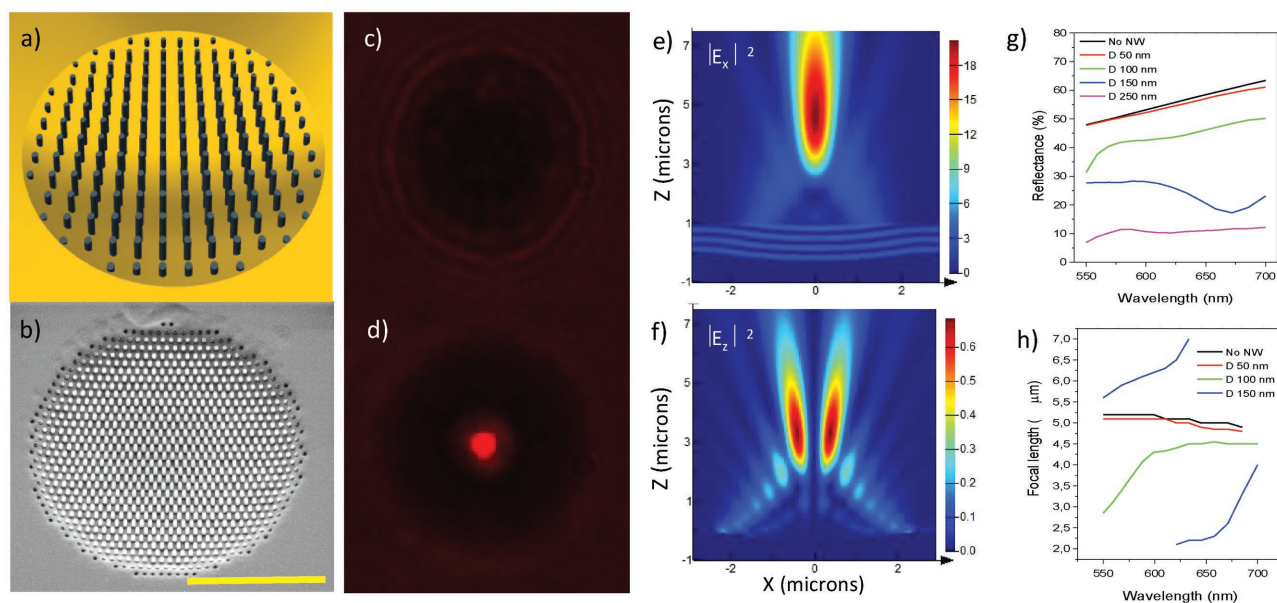


Figure 1. a) Schematic of a circular array of nanowires with height gradient in the radial direction. b) Scanning electron microscopy (SEM) image of a circular array of Si nanowires with height gradients in the radial direction. The array has a diameter of 10 μm , the diameter of the nanowires is 120 nm, the pitch is 300 nm, and their maximum height is 500 nm (the scale bar is 5 μm). c) Optical image of the same array at the surface of the sample. d) Optical image of the focused reflected light by the array of nanowires with radial phase gradient. The focal length is 12 μm . e, f) Theoretical spatial distribution of $|E_x|^2$ and $|E_z|^2$ components of the reflected light by the array of Si nanowires with radial height gradient, respectively. The diameter of the array is 5 μm , the pitch is 300 nm, and the nanowires diameter is 50 nm. The maximum height of the nanowires at the center of the array is 300 nm. g) Theoretical reflectance of the metalenses with nanowire diameters D ranging from 50 to 250 nm compared to that of a silicon spherical mirror with 20 nm gold film. h) Theoretical focal length of the spherical mirror and the metamirrors with D ranging from 50 to 150 nm.

Due to computational limitations given by the large size of the computational volume, the size of the arrays in the calculations is restricted to 5 μm in diameter. Figure 1e,f displays the squared absolute value of the E_x and E_z components of the reflected light assuming an incident plane wave propagating in the z -direction and polarized in the x -direction. The focused spot can be seen in the amplitude of the E_x component of the reflected electromagnetic field, whereas E_z shows two lobes with zero intensity at the axis of the mirror. Since the nanowires have circular symmetry, the reflected light keeps the same polarization plane and the E_y component is zero. Similar focusing effects can also be achieved without the Au film at the bottom, even though the light intensity at the focus and the metamirror reflectance are lower, as can be observed in Figure S1 (Supporting Information).

The diameter of the nanowires plays an important role in the focusing efficiency. The focusing effect is broadband for nanowires with diameter D equal or less than 50 nm, since the absorption by these nanowires is negligible and there are not Mie resonances in the visible range. In these conditions the metamirror focal length barely changes with the light wavelength, and the focal length f is similar to that of a spherical mirror, which is given by

$$f = \frac{R}{2} = \frac{H}{4} + \frac{W^2}{16H} \quad (1)$$

where R is the radius of the spherical mirror, H is the height of the nanowires at the center of the array, and W is the diameter of the array (see the Supporting Information). The focal length

in the calculations of Figure 1e is 5 μm , and the reflectance in the visible is practically equal to that of a spherical mirror (Figure 1g). When the diameter of the nanowires is enlarged, the absorption increases and the Mie resonances, although damped due to the Si substrate, start to show an increasing effect on the reflectance and focal length of the metamirrors. When D is 100 nm, the reflectance reduction at 550 nm wavelength is accompanied by a substantial shortening of the focal length (Figure 1g,h). In contrast, for D equal to 150 nm, this effect is observed at longer wavelengths (≈ 660 nm). Such variations of the focal length are due to the Mie resonance of the Si nanowires (Figure S2, Supporting Information), which redshifts as the D increases. Interestingly, for slightly shorter wavelengths than that of the resonance, there are two focal points at different distance (Figure 1h and Figure S2, Supporting Information). The intensity of the focal point at short distance is rapidly reduced as the incident light wavelength decreases, while the intensity of the focal point at longer distance increases and its focal distance slowly tends to that of the spherical mirror (Figure S2, Supporting Information). In arrays of nanowires with D larger than 200 nm, the reflectance is largely reduced and most of the visible light is absorbed by the array, as can be seen in Figure 1h.

A remarkable feature of the employed nanofabrication technique is its capacity to generate arrays with height gradients in arbitrary directions by changing the shape of the nanoholes array in the catalytic gold mesh.^[21] Such capability is illustrated in Figure 2, where we show ring-shaped arrays of nanowires that focus the light in a ring with focal length of 10 μm . As predicted in the FDTD calculation, ring-shaped

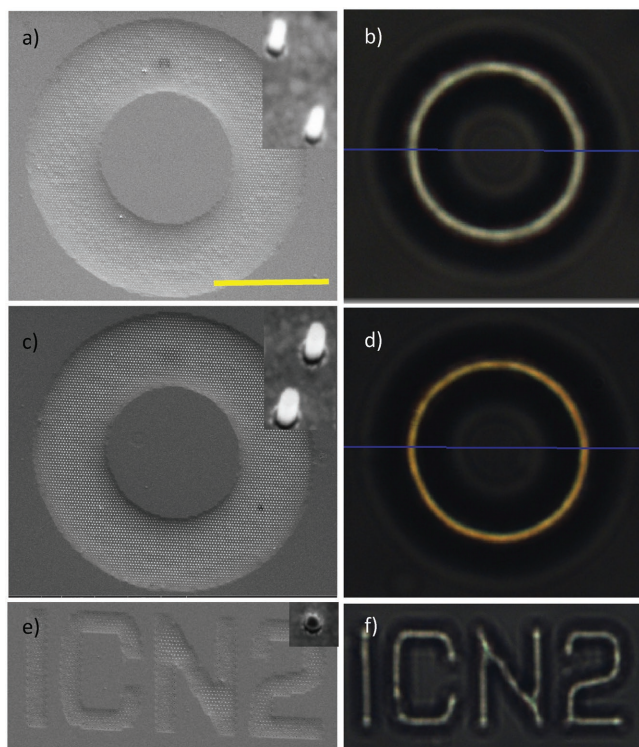


Figure 2. a) SEM images of a ring-shaped metamirror (scale bar 10 μm). The internal and external diameters of the array are 7.5 and 15 μm , respectively, and the diameter of the nanowires is 50 nm and their maximum height is 320 nm. b) Optical image of the focused light by the ring with focal length of 10 μm . c,d) SEM and optical images of a similar ring-shaped metamirror but for a nanowire diameter of 100 nm and a maximum height of 340 nm. e,f) SEM and optical images of ICN2-shaped metamirror showing a focal length of 3 μm . The lateral size of the arrays is 2.5 μm , the nanowires diameter is 150 nm, and their maximum height is 120 nm. The optical images are taken using collimated white light from a halogen lamp.

arrays of 50 nm diameter nanowires present broadband focusing (Figure 2b).

In contrast, when the nanowires diameter is 100 nm, light intensity in the blue spectral range decreases at the focal plane located at 10 μm , which corresponds to the expected focal length of a cylindrical mirror. Such intensity decrease is due to the Mie resonance of the Si nanowires in this spectral region. As a consequence, part of the blue light is absorbed and part is focused at a lower focal plane, thereby yielding the yellow focused ring in Figure 2d. In addition, Figure 2e,f shows how light can be focused in virtually any shape by modifying the geometry of the arrays. Interestingly, these metamirrors with a lateral size of the array of nanowires of 2.5 μm and height variations from zero to 120 nm are able to achieve a focal length as low as 3 μm , thereby demonstrating the capacity to tune both the shape of the focused light and the focal length with the geometry of the metamirror.

All the metamirrors described so far are geometrically isotropic, i.e., the resulting focused light preserves the polarization of the impinging wave. However, the ability to combine nanowires with arbitrary cross sections and height gradients within the arrays opens up the opportunity to exert additional control

on the polarization of the focused light. This is shown in the FDTD calculations of Figure 3a that show intense polarization conversion when the long axis of the nanowires is oriented at 45° with respect to the polarization of incident light. By comparing the intensity of the E_x and E_y components at the focus to that of E_x when the long axes of the nanowires are parallel to the polarization of incident light, a 30% conversion efficiency is predicted at 600 nm light wavelength and close to 20% at 660 nm.

These polarization conversion effects can be experimentally observed in Figure 3b–d, for circular arrays of nanowires with elongated cross section and radial height gradient. When the short or long axes of the nanowires are parallel to the polarization of the incident light, the focused reflected light keeps the same polarization. Consequently, focused spots with slightly different intensities are observed when the analyzer is parallel to the incident light polarization (Figure 3c), but the reflected light is totally blocked when the analyzer is oriented perpendicularly (Figure 3d). In contrast, when the nanowires are aligned at 45° with respect the incident polarization, the focused spot is clearly seen for both orientations of the analyzer, thereby demonstrating the polarization conversion effect. Comparison of the focalized intensity in both analyzer orientations demonstrates that 30% conversion efficiency at 660 nm is experimentally achieved.

In conclusion, we have introduced arrays of silicon nanowires with height gradients as an interesting way to create optical metamaterials capable of light texturing and to develop a new generation of metamirrors able to focus light in complex patterns and, simultaneously, spatially control light polarization. Mechanical transfer of the arrays of Si nanowires to low refractive index substrates could also enable developing metalenses for transmitted light in the visible and infrared. Such metalenses would fully exploit the tunable Mie multipolar resonances and scattering patterns of silicon nanowires,^[24–26] which are strongly damped when they are on a silicon wafer, to achieve stronger lensing effects. Such silicon nanowire metalenses could find remarkable photonic applications. The possibility to fabricate arrays of metalenses with tailored geometries could be employed for efficient light coupling in fiber bundles. Moreover, the demonstrated ability to focus the light in arbitrary shapes with spatially tailored polarization could be applied for light coupling in integrated optical circuits and optical fibers and for the controlled efficient excitation of high order guided modes. Finally, polymer negative replicas of the Si nanowire metamirrors by nanoimprint techniques also offer a low cost alternative for developing new arrays of metalenses with very short focal lengths.

Experimental Section

Fabrication of the Silicon Nanowire Metamirrors: First, a titanium/gold bilayer (0.5 nm/20 nm) was evaporated on top of piranha-cleaned silicon wafers (100) via electron beam deposition, on which a polymethyl methacrylate (PMMA 950 K, 6% in Anisole) resist layer was spin coated (4000 rpm: thickness \approx 300 nm). Then, electron beam lithography (EBL) was used to pattern arrays of nanoholes of different geometries into the resist. After EBL exposure the resist was developed during 40 s in a mixture of methyl isobutyl ketone and isopropyl alcohol (IPA) at a ratio of 1:3. Immersing the chip in IPA stopped the process, and after that it was blown dry with N_2 flow.

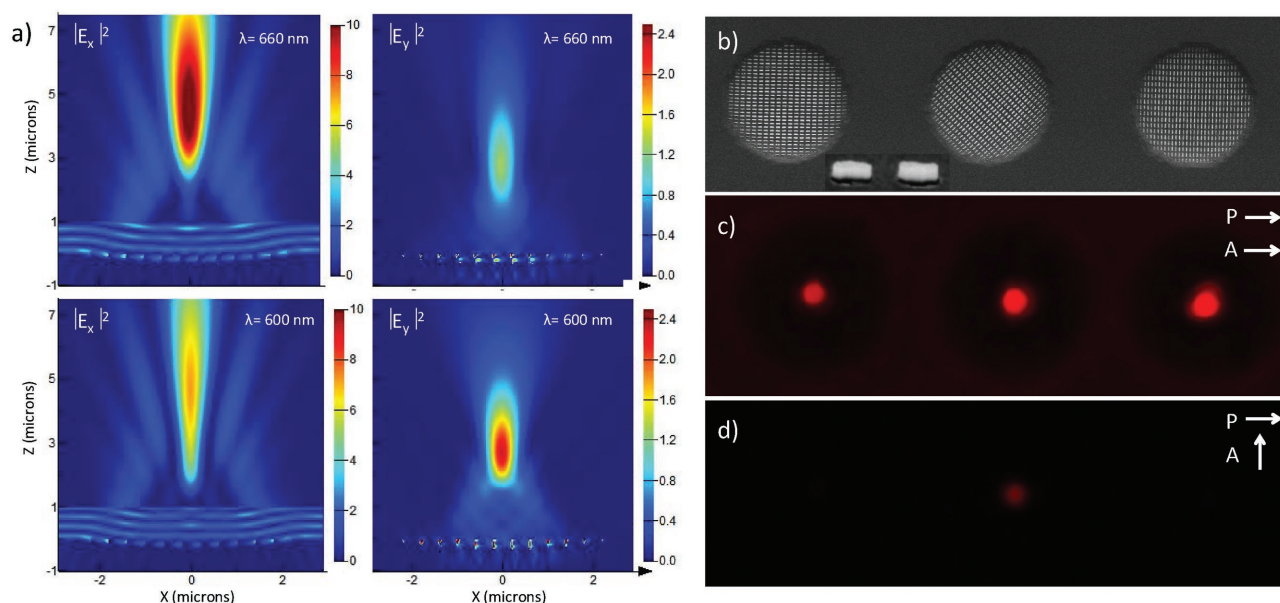


Figure 3. a) FDTD calculations of an anisotropic metamirror formed by an array of nanowires with ellipsoidal cross-section and radial height gradients showing the squared absolute values of E_x and E_y when the incident light is 660 and 600 nm. The short and long axis of the nanowires are 250 and 100 nm, respectively, and are oriented at 45° with respect to light polarization, the array diameter is $5 \mu\text{m}$ and the nanowires height at the center of the array is 300 nm. The pitch parallel and perpendicular to the long axis of the nanowires is 400 and 300 nm, respectively. b) SEM image of circular metamirrors with $10 \mu\text{m}$ diameter and elongated nanowires with the long axis oriented at 0° (left), 45° (center), and 90° (right) with respect to the polarization of the incident light. The long and short axes of the nanowires are 250 and 100 nm, respectively. The pitch in the array is 300 nm parallel to the short axis and 400 nm parallel to the long axis. c) Optical image of the focused light by the arrays when the incident light polarizer P and analyzer A of the reflected light are aligned. The incident light is a collimated 660 nm light beam from an light emitting diode (LED) lamp. d) Optical image of the focused reflected light when the analyzer A is rotated 90° with respect to the incident light polarizer P .

The patterned PMMA layer was used as a mask for the removal of the exposed gold inside the holes by directional argon sputtering treatment (inductively coupled plasma reactive ion Etching (ICP-RIE), power 1000 W, chuck power 25 W, pressure 1 Pa, flow 20 sccm, time 50 s). During this process, the ≈ 300 nm thick PMMA layer was strongly damaged, but it was still sufficiently thick to protect the gold layer underneath. Subsequently, the remaining PMMA was removed via an oxygen reactive ion etching (ICP RIE power 500 W, pressure 1 Pa, flow 20 sccm, time 240 s), leaving a clean, patterned 20 nm thick gold layer.

The silicon nanopillars were finally created via metal-assisted chemical etching (MACE), by immersing the sample into a mixture of H_2O (89.5%), H_2O_2 (0.5%), and hydrofluoric acid (HF; 10%) for 2 min. To stop the MACE, the samples were immersed in water. Finally, the samples were transferred to IPA to minimize capillary effects upon drying with N_2 flow.

Optical Characterization of the Metamirrors: A custom-made optical setup had been used to optically characterize the metamirrors. The sample was mounted on a motorized stage that enabled a controlled variation of the Z distance with the respect to the microscope objective. Additional manual stages were used to move the sample in the XY directions. The light from either a fiber coupled LED (Thorlabs) with central emission wavelength at 660 nm or a halogen lamp (Ocean Optics) was collimated by an achromatic lens, passed through a lineal polarizer and a 50/50 beam splitter, and, using a second achromatic lens, was finally focused on the back focal plane of an ultralong working distance 100X Nikon objective, to achieve collimated light at the output. The reflected light by the sample traveled through a tube lens and a second polarizer (analyzer) and was then captured by a Nikon DFS11 charged-coupled device (CCD) camera. The motorized Z stage enabled focusing the surface of the sample on the CCD camera as well as imaging the focused spots and measuring the focal length of the metamirrors.

FDTD Calculations: The FDTD calculations had been performed using commercial Lumerical software. The mesh resolution in the region of the nanowires and the metal film was 5 nm, and the authors had employed a total field scattered field source incident on the metamirror and perfect matched layer, boundary conditions. To avoid undesired instabilities caused by the metal film at short wavelengths, the calculations of the metamirrors were restricted to the 550–700 nm spectral range.

Supporting Information

Supporting Information is available from the Wiley Online Library or from the author.

Acknowledgements

The authors acknowledge the financial support of the Spanish Ministerio de Economía y Competitividad (MINECO) projects MAT2013-48628-R, FIS2013-49280-EXP, and MAT2011-12645-E and Comunidad the Madrid project S2013/MIT-2740. ICN2 acknowledges support from the Severo Ochoa Program (MINECO, Grant SEV-2013-0295).

Received: November 10, 2016

Revised: December 7, 2016

Published online: January 27, 2017

[1] N. Yu, F. Capasso, *Nat. Mater.* **2014**, *13*, 139.

[2] A. V. Kildishev, A. Boltasseva, V. M. Shalaev, *Science* **2013**, *339*, 1289.

- [3] A. Poddubny, I. Iorsh, P. Belov, Y. Kivshar, *Nat. Photonics* **2013**, *7*, 958.
- [4] A. A. High, R. C. Devlin, A. Dibos, M. Polking, D. S. Wild, J. Perczel, N. P. de Leon, M. D. Lukin, H. Park, *Nature* **2015**, 522, 192.
- [5] R. Maas, J. Parsons, N. Engheta, A. Polman, *Nat. Photonics* **2013**, *7*, 907.
- [6] N. Shitrit, I. Yulevich, E. Maguid, D. Ozeri, D. Veksler, V. Kleiner, E. Hasman, *Science* **2013**, *340*, 724.
- [7] G. Li, M. Kang, S. Chen, S. Zhang, E. Y. Pun, K. W. Cheah, J. Li, *Nano Lett.* **2013**, *13*, 4148.
- [8] E. Karimi, S. A. Schulz, I. De Leon, H. Qassim, J. Upham, R. W. Boyd, *Light: Sci. Appl.* **2014**, *3*, e167.
- [9] X. Yin, Z. Ye, J. Rho, Y. Wang, X. Zhang, *Science* **2013**, *339*, 1405.
- [10] L. Huang, X. Chen, H. Mühlenbernd, H. Zhang, S. Chen, B. Bai, Q. Tan, G. Jin, K. Cheah, C. Qiu, J. Li, T. Zentgraf, S. Zhang, *Nat. Commun.* **2013**, *4*, 2808.
- [11] G. Zheng, H. Mühlenbernd, M. Kenney, G. Li, T. Zentgraf, S. Zhang, *Nat. Nanotechnol.* **2015**, *10*, 308.
- [12] N. Yu, F. Aieta, P. Genevet, M. A. Kats, Z. Gaburro, F. Capasso, *Nano Lett.* **2012**, *12*, 6328.
- [13] N. Yu, P. Genevet, M. A. Kats, F. Aieta, J. Tetienne, F. Capasso, Z. Gaburro, *Science* **2011**, *334*, 333.
- [14] S. Sun, Q. He, S. Xiao, Q. Xu, X. Li, L. Zhou, *Nat. Mater.* **2012**, *11*, 426.
- [15] X. Ni, S. Ishii, A. V. Kildishev, V. M. Shalaev, *Light: Sci. Appl.* **2013**, *2*, e72.
- [16] S. Ishii, V. M. Shalaev, A. V. Kildishev, *Nano Lett.* **2013**, *13*, 159.
- [17] A. García-Etxarri, R. Gómez-Medina, L. S. Froufe-Pérez, C. López, L. Chantada, F. Scheffold, J. Aizpurua, M. Nieto-Vesperinas, J. J. Sáenz, *Opt. Express* **2011**, *19*, 4815.
- [18] N. de Sousa, L. S. Froufe-Pérez, J. J. Sáenz, A. García-Martín, *Sci. Rep.* **2011**, *6*, 30803.
- [19] D. Lin, P. Fan, E. Hasman, M. L. Brongersma, *Science* **2014**, *345*, 6194.
- [20] F. Aieta, M. A. Kats, P. Genevet, F. Capasso, *Science* **2015**, *347*, 1342.
- [21] Y. Xu, Y. Fu, H. Chen, *Nat. Rev. Mater.* **2016**, *1*, 16067.
- [22] A. E. Minovich, A. E. Miroschnichenko, A. Y. Bykov, T. V. Murzina, D. N. Neshev, Y. S. Kivshar, *Laser Photonics Rev.* **2015**, *9*, 195.
- [23] M. A. Otte, V. Solis-Tinoco, P. Prieto, X. Borrísé, L. M. Lechuga, M. U. González, B. Sepulveda, *Small* **2015**, *11*, 4201.
- [24] M. Nieto-Vesperinas, R. Gomez-Medina, J. J. Saenz, *J. Opt. Soc. Am. A* **2011**, *28*, 54.
- [25] J. M. Geffrin, B. García-Cámara, R. Gómez-Medina, P. Albella, L. S. Froufe-Pérez, C. Eyraud, A. Litman, R. Vaillon, F. González, M. Nieto-Vesperinas, J. J. Sáenz, F. Moreno, *Nat. Commun.* **2012**, *3*, 1171.
- [26] B. García-Cámara, R. Gómez-Medina, J. J. Sáenz, B. Sepúlveda, *Opt. Express* **2013**, *21*, 23007.